Fourier-Laplace Spectral Theory for Non-Steady-State Thermal Fields with Applications to Problems in Steady-State Photothermal Linear Frequency Modulation

Andreas Mandelis* and Xinxin Guo

Center for Advanced Diffusion-Wave and Photoacoustic Technologies (CADIPT), Department of Mechanical and Industrial Engineering, University of Toronto, Toronto, Ontario M5S 3G8, Canada

(Received 20 April 2020; revised 9 June 2020; accepted 20 July 2020; published 20 August 2020)

The spectral theory of thermal fields subject to arbitrary boundary surface flux conditions developed in this work establishes a universal approach to non-steady-state (photo)thermal responses of solids under transient or modulated thermal excitation through a combined Fourier-Laplace formalism. The self-consistent evolution from the nonsteady state to the steady state under single frequency or arbitrary pulsed or multifrequency thermal-wave excitation waveforms allows for defining experimental criteria in terms of excitation waveform repetition periods to attain steady state in frequency-modulated photothermal (and other general experimental) systems. This approach is crucial for ensuring accurate material property measurements using lock-in or correlation and spectral analysis demodulation of thermal waves, especially under linear frequency modulation (LFM) when the modulated steady state is time dependent. The theory is validated using experimental photothermal radiometry LFM responses from black anodized aluminum. We also define the associated thermal diffusion length in terms of linear superpositions of partial thermal waves (wavelets), which are shown to result in improved depth, lateral, and axial resolution in thermal-wave radar imaging applications compared with sequential single-modulation frequency detection.

DOI: 10.1103/PhysRevApplied.14.024058

I. INTRODUCTION

Over the past five decades, thermal-wave theory has evolved mainly along the lines of the various experimental modalities developed by research groups around the world, with the primary motivator being the application of thermal waves to photoacoustic spectroscopy and related photothermal detection techniques. From the onset of the modern-day renaissance of the field of condensed matter photoacoustics in the 1970s, two major signal-generation and -detection modalities emerged as discrete branches along with the associated theoretical analyses: frequency domain [1,2] and time domain [3]. Early books by Pao [4] and Rosencwaig [5] gave an excellent account of the (photo)thermal analyses associated with pioneering experiments, in which the thermal component of the signal dominated the system response. McDonald and Wetsel refined the theory by coupling acoustic contributions to the frequency-domain signal [2]. The later landmark book by Gusev and Karabutov on laser-induced time-domain photoacoustics [6] presented details of the ultrasonic aspects of the field, in step with the rapid development of laser ultrasonic applications to condensed matter physics and engineering. A (photo)thermal signal-generation modality intermediate between the time and frequency domain appeared in the 1980s [7–9] based on linear frequency modulation (LFM) chirps, correlation, and spectral analysis. This modality has evolved into the concept of the thermal-wave radar [10] and related approaches [11] and has resulted in the recent rapid growth of dynamic infrared thermal imaging using pulse compression and match filtering [12–16]. Several theoretical attempts have been made to quantify time-dependent LFM-chirp-based thermal-wave signals with approximate [11,17,18] approaches to the associated generalized boundary-value problem that appear to be extensions of the conventional single-frequency thermal-wave approaches [19], yet, a rigorous approach to the generalized time- and multifrequency modulation problem is lacking. The present investigation addresses the generalized theory of hybrid time-frequency domain thermal-wave fields with arbitrary temporal excitation sources, applications to purely time- and frequency-domain case studies, and special focus on LFM excitation. The major outcome of the generalized theory is the insight that the barrier to deriving exact solutions to multifrequency thermal waves is directly associated with the presence of *non-steady-state* modulation, unlike the conventional time-domain thermal field responses (transients with absence of modulation) or the harmonically modulated thermal-wave fields (steady-state modulation).

*mandelis@mie.utoronto.ca

II. FOURIER-LAPLACE SPECTRAL THEORY OF ONE-DIMENSIONAL THERMAL FIELDS

To minimize complexities due to multidimensional solid geometries, a one-dimensional solid is considered, subject to thermal excitation by an arbitrary (photo)thermal flux $f(t)$ on its surface. The boundary-value problem under consideration is described by the conventional diffusion equation:

$$\frac{\partial^2\theta(x,t)}{\partial x^2}-\frac{1}{\alpha}\frac{\partial\theta(x,t)}{\partial t}=0;\quad t\geq 0,\quad 0\leq x\leq L, \tag{1}$$

subject to the arbitrary-flux boundary condition

$$-k\frac{\partial\theta(x,t)}{\partial x}|_{x=0}=f(t), \tag{2}$$

where $\theta(x,t)$ is the generalized temperature field (thermal wave, in the case of modulated input), and α and k are the material thermal diffusivity and conductivity, respectively. Equation (1) can be solved by means of separation of variables

$$\theta(x,t)=X(x)T(t). \tag{3}$$

Given that hybrid domain analysis requires access to both frequency- and time-domain characteristics, we introduce a combined Fourier-Laplace approach that leads to spectral decomposition of the resulting thermal field. It requires an imaginary separation constant, $i\lambda^2=i\omega$, so that the thermal field is described as a Fourier superposition of all its spectral (frequency) elements:

$$\theta(x,t)=\frac{1}{2}\int_{-\infty}^{\infty}C(\omega)X(x;\omega)e^{i\omega t}\frac{d\omega}{\sqrt{\omega}}, \tag{4}$$

subject to the transformed boundary condition of Eq. (2):

$$\int_{-\infty}^{\infty}C(\omega)\left[\frac{dX(x;\omega)}{dx}|_{x=0}\right]e^{i\omega t}\frac{d\omega}{\sqrt{\omega}}=-\frac{2}{k}f(t). \tag{5}$$

Introducing the definition of a Fourier transform pair

$$g(t)=\int_{-\infty}^{\infty}\tilde{G}(\omega)e^{i\omega t}d\omega, \tag{6a}$$

$$\tilde{G}(\omega)=\frac{1}{2\pi}\int_{-\infty}^{\infty}g(t)e^{-i\omega t}dt, \tag{6b}$$

and in view of Eq. (4), Eqs. (5) and (6) yield

$$C(\omega)=\frac{\sqrt{\omega}\int_{-\infty}^{\infty}g(t)e^{-i\omega t}dt}{2\pi[dX(x;\omega)/dx|_{x=0}]}, \tag{7a}$$

with

$$\tilde{G}(x;\omega)=\frac{1}{2\pi}\frac{X(x;\omega)}{[dX(x;\omega)/dx|_{x=0}]}, \tag{7b}$$

where the argument of the response function, $g(t)$, of the solid in Eq. (6a) is written to explicitly show its dependence on the x coordinate, so that $\tilde{G}=\tilde{G}(x;\omega)$. Substituting Eq. (7) into Eq. (4) and using $g(t)=(-2/k)f(t)$ from Eq. (5) gives the generalized thermal field in terms of the Fourier transform of the incident surface flux:

$$\theta(x,t)=-\frac{1}{k}\int_{-\infty}^{\infty}\tilde{F}(\omega)\left\{\frac{X(x;\omega)}{[dX(x;\omega)/dx|_{x=0}]}\right\}e^{i\omega t}d\omega, \tag{8a}$$

where

$$\tilde{F}(\omega)=\frac{1}{2\pi}\int_{-\infty}^{\infty}f(t)e^{-i\omega t}dt, \tag{8b}$$

is the frequency spectrum of the incident time-dependent (photo)thermal flux. For the general one-dimensional geometry of a solid with finite thickness L, the function $X(x;\omega)$ in Eq. (3) takes on the meaning of the spatial distribution of the spectrum $\{\omega\}$ of the temperature $\theta(x,t)$:

$$\frac{d^2X(x;\omega)}{dx^2}-\left(\frac{i\omega}{\alpha}\right)X(x;\omega)=0. \tag{9}$$

The general solution of Eq. (9) is

$$X(x;\omega)=K_1(\omega)\exp[(i\omega/\alpha)^{1/2}x]+K_2(\omega)\exp[-(i\omega/\alpha)^{1/2}x]. \tag{10}$$

K_1 and K_2 are integration constants and are determined by suitable boundary conditions at $x=0$, L. From Eqs. (7b) and (10), the frequency spectrum of the *response* of the general solid to the incident flux is expressed as

$$\tilde{G}(x;\omega)=\frac{K_1(\omega)\exp[(i\omega/\alpha)^{1/2}x]+K_2(\omega)\exp[-(i\omega/\alpha)^{1/2}x]}{(i\omega/\alpha)^{1/2}[K_1(\omega)-K_2(\omega)]}. \tag{11}$$

Equations (7b) and (8) show that the spectrum (Fourier transform) of the temperature field is the product of the

spectra of the incident flux and the solid response:

$$\theta(x,t) = -\frac{1}{k}\int_{-\infty}^{\infty} \tilde{F}(\omega)\tilde{G}(x;\omega)e^{i\omega t}d\omega. \tag{12}$$

Invoking the Fourier convolution theorem, Eq. (12) becomes

$$\theta(x,t) = -\frac{1}{k}f\,(t)g(x,t) = -\frac{1}{k}\int_{-\infty}^{\infty} f\,(t-\tau)g(x,\tau)d\tau. \tag{13}$$

For the case of a semi-infinite solid, $K_1(\omega) = 0$ in Eq. (11) and the temperature field takes on the simplified form

$$\theta(x,t) = \frac{1}{2\pi k}\int_{-\infty}^{\infty} \tilde{F}(\omega)\left[\frac{e^{-(i\omega/\alpha)^{1/2}x}}{(i\omega/\alpha)^{1/2}}\right]e^{i\omega t}d\omega. \tag{14}$$

It is instructive to note that the convolution of Eq. (13) with $g(x,t)$ as the inverse Fourier transform of the expression in brackets in Eq. (14) is the spectral-domain counterpart of the Laplace domain formula for a semi-infinite solid with zero initial temperature and subject to an arbitrary time-dependent heat flux, $f\,(t)$, at $x = 0$:

$$\theta(x,t) = \frac{1}{k}\sqrt{\frac{\alpha}{\pi}}\int_0^t f\,(t-\tau)\left[\frac{e^{-(x^2/4\alpha\tau)}}{\sqrt{\tau}}\right]d\tau. \tag{15}$$

Equation (15) was presented by Carslaw and Jaeger [20] as a derivation from Duhamel's theorem. The apparent correspondence is significant because it bridges the Fourier frequency spectrum and the Laplace time-domain approaches. In the Fourier-Laplace approach, to ensure convergence of the integral in Eq. (14), the Fourier transform of the temperature field is multiplied by the Heaviside function, $H(t)$, and a complex Fourier variable, $p = c + i\omega$, is introduced [21], where c is a real constant >0 to the right of all poles and singularities on the real axis of the inverse Laplace-Bromwich contour in the complex plane

$$\begin{aligned}\tilde{\Theta}(x;\omega) &= \int_{-\infty}^{\infty} \theta(x,t)H(t)e^{-(c+i\omega)t}dt \\ &= \int_0^{\infty} \theta(x,t)e^{-(c+i\omega)t}dt,\end{aligned} \tag{16}$$

This transformation from Fourier to Laplace inversion formalism confirms the fact that $\theta(x,t)$ is a time-domain field defined for $t \geq 0$ and synthesized from its frequency spectrum, with the spectral integral of Eq. (14) being converted into a complex Laplace inversion integral

$$\theta(x,t) = \frac{1}{2\pi ik}\int_{c-i\infty}^{c+i\infty} \tilde{F}(p)\tilde{G}(x;p)e^{pt}dp, \tag{17}$$

with the Laplace-transformed response function

$$\tilde{G}(x;\omega) \rightarrow \tilde{G}(x;p) = \sqrt{\alpha}\left[\frac{e^{-(x/\sqrt{a})\sqrt{p}}}{\sqrt{p}}\right]. \tag{18}$$

This thermal kernel function has the well-known inverse Laplace transform

$$g(x,t) = \mathcal{L}^{-1}[\tilde{G}(x;p)] = \sqrt{\frac{\alpha}{\pi t}}e^{-x^2/4\alpha t}, \tag{19}$$

which renders the Fourier convolution of Eq. (13) equivalent to the Laplace convolution of Eq. (15). This type of Fourier- and Laplace-transformed formalism equivalence to time-domain problems has conventionally been assumed to be universal [21,22], with the only possible differences being in the domain of validity and existence of the pertinent integrals. In the following applications and special cases, it is seen that the equivalence breaks down in the case of modulated non-steady-state thermal-wave fields.

III. SPECIAL CASES OF FOURIER-LAPLACE NON-STEADY-STATE (PHOTO)THERMAL RESPONSES OF SEMI-INFINITE SOLIDS

A. Thermal impulse on the surface of a semi-infinite solid

The important case of a thermal impulse source is described by the Dirac delta function:

$$f\,(t) = F_0\delta(t). \tag{20}$$

In Eq. (17), we set $\tilde{F}(p) = F_0$. Using Eqs. (18) and (19), the temperature field expression yields the well-known time-domain transient result:

$$\begin{aligned}\theta(x,t) &= \frac{F_0\sqrt{\alpha}}{2\pi ik}\int_{c-i\infty}^{c+i\infty}\left[\frac{e^{-(x/\sqrt{\alpha})\sqrt{p}}}{\sqrt{p}}\right]e^{pt}dp \\ &= \left(\frac{F_0\sqrt{\alpha}}{k\sqrt{\pi t}}\right)e^{-x^2/4\alpha t}; \quad t > 0.\end{aligned} \tag{21}$$

It should be noted that no field modulation is assumed for this type of excitation. An interesting transient modulation case arises from application to truncated correlation photothermal coherence tomography [14], which, albeit relevant to this theory, is nevertheless outside the scope of the present investigation. The thermal diffusion length

(TDL) represents the thermal mass centroid of the spatial field distribution Eq. (21). In its most generalized form, it is defined as

$$\langle x(t)\rangle = \frac{\int_0^\infty x|\theta(x,t)|dx}{\int_0^\infty |\theta(x,t)|dx}. \tag{22}$$

In the case where the function $\theta(x,t)$ in the integrand is a temporal (real) transient, Eq. (21), the absolute value signs are omitted and this definition yields the time-dependent TDL:

$$\langle x(t)\rangle = 2\sqrt{\frac{\alpha t}{\pi}}, \tag{23}$$

which exhibits the well-known monotonic increase with the square root of time.

B. Fixed-frequency modulation waveform

1. Non-steady-state single-frequency thermal waves

This is the conventional harmonic thermal excitation of the surface of an opaque solid, which is the simplest form of modulation at angular frequency $\omega_0 = 2\pi f_0$. The thermal-wave flux is described by

$$f(t) = \frac{1}{2}F_0(1+e^{i\omega_0 t})H(t); \quad 0 \le t < \infty. \tag{24}$$

Using the Fourier-Laplace approach with Eq. (18) for the solid-material response term and the Laplace transform of Eq. (24) given by

$$\tilde{F}(p) = \frac{1}{2}F_0\left(\frac{1}{p} + \frac{1}{p-i\omega_0}\right), \tag{25}$$

substitution in Eq. (17) and inverse Laplace transformation yields the *non-steady-state* thermal-wave field expression

$$\theta(x,t;\omega_0) = \frac{F_0\sqrt{\alpha}}{2k}\left[2\sqrt{t}i\mathrm{erfc}\left(\frac{x}{2\sqrt{\alpha t}}\right) + \frac{1}{2\sqrt{\omega_0}}\left\{e^{-\sqrt{i\omega_0/\alpha}x}\mathrm{erfc}[z_-(x,t)] - e^{\sqrt{i\omega_0/\alpha}x}\mathrm{erfc}[z_+(x,t)]\right\}e^{i\left(\omega_0 t-\frac{\pi}{4}\right)}\right], \tag{26a}$$

where

$$\mathrm{erfc}(z) = \frac{2}{\sqrt{\pi}}\int_z^\infty e^{-y^2}dy, \tag{26b}$$

$$i\mathrm{erfc}(z) = \int_z^\infty \mathrm{erfc}(y)dy = \frac{1}{\sqrt{\pi}}e^{-z^2} - z\mathrm{erfc}(z), \tag{26c}$$

$$z_\pm(x,t) \equiv \frac{x}{2\sqrt{\alpha t}} \pm \sqrt{i\omega_0 t}. \tag{26d}$$

We observe that Eq. (26a) exhibits two trends originating in the dc and time-modulated flux components of modulation Eq. (24), respectively: a purely transient behavior described by the first term on the right-hand side and a combined transient-modulated (non-steady-state) behavior described by the remaining two terms. Ignoring the transient term, the remaining thermal-wave terms can be written compactly as

$$\theta(x,t;\omega_0) = \frac{F_0\sqrt{\alpha}}{4k\sqrt{\omega_0}}\{W[z_-(x,t)] - W[z_+(x,t)]\}e^{-\left(\frac{x^2}{4\alpha t}+i\frac{\pi}{4}\right)}, \tag{27}$$

where

$$W(z) \equiv \exp(z^2)\mathrm{erfc}(z). \tag{28}$$

Equation (28) describes non-steady-state modulation of the (photo)thermal field. It is apparent that, for large values of the arguments, $z_\pm(x,t)$, such that $t \gg t_\infty(x,\omega_0) \equiv \max[(1/\omega_0),(x^2/4\alpha)]$, the complementary error functions in Eq. (26a) tend to the limiting values $\mathrm{erfc}[z_+(x,t)] \to \mathrm{erfc}(\infty) \approx 0$ and $\mathrm{erfc}[z_-(x,t)] \to \mathrm{erfc}(-\infty) \approx 2$. In those limits, the modulated part of Eq. (26a) becomes

$$\theta(x, t \gg t_\infty) = \frac{F_0\sqrt{\alpha}}{2k\sqrt{\omega_0}}e^{-(i\omega_0/\alpha)^{1/2}x}e^{i(\omega_0 t-\pi/4)}. \tag{29}$$

Equation (29) is identical to the well-known modulated *steady-state* thermal-wave field in a semi-infinite solid, Eq. (2.11) in Ref. [19]. The surface value of the non-steady-state modulated field is immediately derived from Eq. (26a):

$$\theta(0,t) = \frac{F_0\sqrt{\alpha}}{2k\sqrt{\omega_0}}e^{i(\omega_0 t-\pi/4)}\mathrm{erf}\left(\sqrt{i\omega_0 t}\right), \tag{30}$$

where the identity

$$\mathrm{erfc}\left(-\sqrt{i\omega_0 t}\right) - \mathrm{erfc}\left(\sqrt{i\omega_0 t}\right) = 2\mathrm{erf}\left(\sqrt{i\omega_0 t}\right);$$
$$\mathrm{erf}(z) = \frac{2}{\sqrt{\pi}}\int_0^z e^{-y^2}dy, \tag{31}$$

can be easily proven and is used in Eq. (30). In the limit of $t \gg t_\infty(0,\omega_0) = 1/\omega_0$, $\mathrm{erf}\left(\sqrt{i\omega_0 t}\right) \to \mathrm{erf}(\infty) \approx 1$, in which case Eq. (30) becomes the well-known expression for the thermal-wave field on the surface of the semi-infinite solid [19]. The TDL of the steady-state modulated

field is given by inserting Eq. (29) into Eq. (22), with the result being

$$\langle x(\omega_0)\rangle = \sqrt{2\alpha/\omega_0}. \tag{32}$$

This is a well-known and widely used expression [1,20]. However, if the entire combined transient and non-steady-state expression (26a) is used in the limit $t \gg t_\infty(x,\omega_0)$, it is found that $\langle x\ (t\to\infty)\rangle \to (4\sqrt{\alpha t}/3\sqrt{\pi})$, which is a TDL dominated by the ever-growing transient term alone. This occurs because the modulated component of the diffusion length becomes negligible at times $t \gg t_\infty(x,\omega_0)$, compared with the transient TDL, thereby indicating that the Fourier-Laplace formalism is not suitable for modeling the steady-state behavior of modulated thermal waves. Nevertheless, this formalism is useful in describing the intermediate (non-steady-state) behavior of a pure sinusoidal thermal wave and the time-dependent components (both transient and modulated) of the diffusion length.

2. Steady-state single-frequency thermal waves

The derivation of the steady-state modulated thermal-wave response from the assumed semi-infinite solid becomes much simpler when the Fourier approach is adopted. Neglecting the dc term of the flux modulation in Eq. (25) and recalling the Dirac delta function definition

$$\delta(\omega) = \frac{1}{2\pi}\int_{-\infty}^{\infty} e^{-i\omega t}dt, \tag{33}$$

Equation (8b) gives the frequency spectrum of the thermal wave

$$\tilde{F}(\omega) = \frac{1}{2}F_0\delta(\omega-\omega_0). \tag{34}$$

When inserted into the spectral integral of Eq. (14), this single-element spectrum immediately yields the expected steady-state thermal-wave expression [19], Eq. (29). The reason for the very different behaviors of the Fourier and Fourier-Laplace approaches, with respect to steady-state calculations, lies in the fact that, despite the periodic nature of the assumed thermal-wave excitation function, the Fourier integral is defined in the limit of infinite period, i.e., it is fundamentally aperiodic. The Fourier-Laplace integral tracks the spectral component evolution of, and the total energy imparted into, the thermal field at all intermediate times, regardless of the periodically modulated energy input. On the contrary, the Fourier integral is insensitive to the intermediate states and directly yields the modulated component of the thermal field at steady state, which is defined at the limit $t\to\infty$. Nevertheless, the use of the Fourier-Laplace approach is valuable for purposes of physical intuition into the temporal evolution of material responses and material's property measurement accuracy when probed by thermal (and other) wavefields: It predicts the relationships between time, space, and frequency parameters that must be satisfied for the steady state to be attained. This is crucial knowledge for periodic excitation flux waveforms when using one (multiple) periods that is (are) short relative to the attainment of steady state and represents a major focus of the present analysis.

C. Multifrequency-modulated periodic thermal waveforms

1. Non-steady-state multifrequency thermal waves

Periodic modulated thermal fluxes on the surface of solids can be described as

$$F(t) = \sum_{n=0}^{\infty} f\ (t-nT_0); \quad 0 \le t \le T_0. \tag{35}$$

The Laplace transform of this periodic excitation is

$$\tilde{F}(p) = \sum_{n=0}^{\infty}\int_{nT_0}^{(n+1)T_0} f\ (t-nT_0)e^{-pt}dt = \frac{\tilde{J}(p)}{1-e^{-pT_0}}, \tag{36a}$$

where

$$\tilde{J}(p) \equiv \int_0^{T_0} f\ (t)e^{-pt}dt, \tag{36b}$$

so that the thermal-wave field in Eq. (17) with a periodic source function or waveform is written as

$$\theta(x,t) = \frac{1}{2\pi i k}\int_{c-i\infty}^{c+i\infty}\left[\frac{\tilde{J}(p)\tilde{G}(x;p)}{1-e^{-pT_0}}\right]e^{pt}dp. \tag{37}$$

Using the Cauchy integral theorem of complex calculus, contributions from the poles in the denominator of the integrand can be found at values of p such that

$$1-e^{-pT_0} = 0 \Rightarrow p = p_n = \frac{2\pi i n}{T_0} \equiv in\omega_0; \quad n = 1,\ 2,\ 3,\ldots, \tag{38}$$

where $\omega_0 = 2\pi/T_0$ is the waveform-repetition angular frequency (rate). The function $\tilde{F}(p)$ in Eq. (36a) can then be calculated in terms of the residues at p_n by

$$\tilde{F}(p_n) = \frac{\tilde{J}(p_n)}{T_0} = \frac{1}{T_0}\tilde{J}(in\omega_0). \tag{39}$$

Finally, invoking the residue theorem with simple poles at p_n gives

$$f(t) = \mathcal{L}^{-1}[\tilde{F}(p)] = \sum_{n=1}^{N} Res[e^{pt}\tilde{F}(p); p = p_n]$$
$$= \frac{1}{T_0}\sum_{n=1}^{\infty}\tilde{J}(in\omega_0)e^{in\omega_0 t} \equiv \sum_{n=1}^{\infty} A_n(\omega_0)e^{in\omega_0 t}. \quad (40)$$

Here, N is the number of isolated singularities in the inverse Laplace complex contour to the left of c on the real (x) axis, and $A_n(\omega_0)$ takes on the definition of the coefficient of the complex Fourier-Laplace series in Eq. (40) of the periodic source function $f(t)$, as given by

$$A_n(\omega_0) = \frac{1}{T_0}\tilde{J}(in\omega_0) = \frac{1}{T_0}\int_0^{T_0} f(t)e^{-in\omega_0 t}dt. \quad (41)$$

In the special case where the periodic (photo)thermal flux waveform is a LFM sweep (chirp) sweeping between angular modulation frequencies ω_1 and ω_2

$$f_{T_0}(t) = \frac{1}{2}F_0 e^{i\omega(t)t}; \quad 0 \le t \le T_0, \quad (42a)$$

with

$$\omega(t) = \omega_1 + \left(\frac{d\omega}{dt}\right)t \equiv \omega_1 + R^2 t; \quad R^2 = \frac{\omega_2 - \omega_1}{2T_0} \equiv \frac{\Delta\omega}{2T_0}, \quad (42b)$$

Equation (41) gives the periodic thermal flux $F(t)$ Fourier-Laplace expansion coefficient

$$A_n(\omega_0) = \frac{F_0}{2T_0}\int_0^{T_0} \exp\{i[R^2t^2 + (\omega_1 - n\omega_0)t]\}dt. \quad (43)$$

An integrand variable change and use of the Fresnel cosine, $C(u)$, and sine, $S(u)$, integrals compactly defined as

$$\left(\frac{2}{\pi}\right)^{1/2}\int_0^u e^{iy^2}dy \equiv C(u) + iS(u), \quad (44)$$

yields the following explicit expression for the complex coefficient A_n:

$$A_n(\omega_0) = \left(\frac{\sqrt{\pi}F_0}{2\sqrt{2}RT_0}\right)\exp\{-i[(n\omega_0 - \omega_1)/2R]^2\}$$
$$\times (C[RT_0 - (n\omega_0 - \omega_1)/2R]$$
$$+ C[(n\omega_0 - \omega_1)/2R]$$
$$+ i\{S[RT_0 - (n\omega_0 - \omega_1)/2R]$$
$$+ S[(n\omega_0 - \omega_1)/2R]\}). \quad (45)$$

Returning to the general multifrequency-modulated thermal-waveform excitation, the derivation of the periodic temperature, $\theta(x,t)$, in a semi-infinite solid requires the use of the thermal-wave kernel function, $\tilde{G}(x,p)$, from Eq. (18) in Eq. (37). This does not lead to a straightforward analysis because the series representation, in terms of simple poles of the periodic flux function $F(t)$, is complicated by the presence of the branch point at the origin introduced by the thermal kernel function, $\tilde{G}(x,p)$, for the semi-infinite solid. Nevertheless, we can perform the inversion by means of the following operations: (1) the simpler thermal kernel function, $\tilde{G}_0(x;p) = e^{-(x/\sqrt{\alpha})\sqrt{p}}$, with known inverse transform is introduced, so that Eq. (37) gives the zeroth-order thermal-wave field

$$\theta_0(x,t) = \frac{1}{2\pi ik}\int_{c-i\infty}^{c+i\infty}\left[\frac{\tilde{J}(p)\tilde{G}_0(x;p)}{1 - e^{-pT_0}}\right]e^{pt}dp; \quad (46)$$

(2) next, the convolution of the inverse of $\tilde{G}_0(x,p)$ with the unit function $h(t) = 1$ is calculated; this introduces a factor of p to the denominator of the integrand in Eq. (46); and (3) finally, the derivative of the Laplace transform of the convolution with respect to $Q(x) = x/\sqrt{\alpha}$ is taken to restore the entire function $\tilde{G}(x,p)$ in the integrand of Eq. (37).

We start with the kernel of Eq. (46)

$$\tilde{K}(x;p) = \frac{1}{k}\left[\frac{\tilde{J}(p)}{1 - e^{-pT_0}}\right]e^{-Q(x)\sqrt{p}}. \quad (47)$$

In which the inverse Laplace transform of the expression in brackets is given by the Fourier-Laplace series in Eq. (40). The remaining term readily yields [23] the inverse Laplace transform

$$\mathcal{L}^{-1}\left[e^{-Q(x)\sqrt{p}}\right] = \frac{Q(x)}{2\sqrt{\pi t^3}}e^{-Q^2(x)/4t} \equiv g_0(x,t). \quad (48)$$

The inverse of the product of these two Laplace transforms gives the convolution integral

$$\mathcal{L}^{-1}[\tilde{K}(x;p)] = f_{T_0}(t) * g_0(x,t) = \int_0^t f_{T_0}(t-\tau)g_0(x,\tau)d\tau$$
$$= K(x,t). \quad (49)$$

Next, we use Laplace-Fourier expansion (40) for the periodic function with coefficients A_n given by Eq. (45), which produces the following series expression for the inverse kernel, K:

$$K(x,t) = \frac{F_0 Q(x)}{4\sqrt{\pi}k}\sum_{n=1}^{\infty}A_n(\omega_0)e^{in\omega_0 t}\int_0^t\left(\frac{d\tau}{\tau^{3/2}}\right)$$
$$\times \exp\left[-\left(\frac{Q^2(x)}{4\tau} + in\omega_0\tau\right)\right]; \quad 0 \le t \le T_0. \quad (50)$$

This integral is reduced to an analytical representation [24], which inverts the zeroth-order thermal-wave field, Eq. (46):

$$\theta_0(x,t)=\frac{F_0}{4k}\sum_{n=1}^{\infty}A_n(\omega_0)e^{in\omega_0 t}\left\{e^{\sqrt{in\omega_0}Q(x)}\mathrm{erfc}\left[\frac{Q(x)}{2\sqrt{t}}+\sqrt{in\omega_0 t}\right]+e^{-\sqrt{in\omega_o t}Q(x)}\mathrm{erfc}\left[\frac{Q(x)}{2\sqrt{t}}-\sqrt{in\omega_0 t}\right]\right\}. \tag{51}$$

For step (2), the convolution of $\theta_0(x,t)$ with the unit function $h(t)$ is determined, such that

$$\mathcal{L}^{-1}[\tilde{H}(p)\tilde{K}(x;p)]=\frac{1}{k}\mathcal{L}^{-1}\left[\frac{\tilde{J}(p)e^{-Q\sqrt{p}}}{p(1-e^{-pT_0})}\right]=h(t)*\theta_0(x,t)=\int_0^t\theta_0(x,\tau)d\tau. \tag{52}$$

Insertion of Eq. (51) into this integral gives

$$h(t)*\theta_0(x,t)=\frac{F_0}{4k}\sum_{n=1}^{\infty}A_n(\omega_0)\left[e^{\sqrt{in\omega_0}Q}I_+^{(n)}(Q,t)+e^{-\sqrt{in\omega_0}Q}I_-^{(n)}(Q,t)\right], \tag{53}$$

where the following integrals appear and can be evaluated analytically using by-parts integration and Leibniz's rule:

$$\begin{aligned}I_\pm^{(n)}(Q,t)&=\int_0^t e^{in\omega_0\tau}\mathrm{erfc}\left(\frac{Q}{2\sqrt{\tau}}\pm\sqrt{in\omega_0\tau}\right)d\tau\\&=\frac{1}{in\omega_0}\left[e^{in\omega_0 t}\mathrm{erfc}\left(\frac{Q}{2\sqrt{t}}\pm\sqrt{in\omega_0 t}\right)-e^{\mp\sqrt{in\omega_0}Q}\mathrm{erfc}\left(\frac{Q}{2\sqrt{t}}\right)\pm 2\sqrt{in\omega_0 t}e^{\mp\sqrt{in\omega_0}Q}i\mathrm{erfc}\left(\frac{Q}{2\sqrt{t}}\right)\right].\end{aligned} \tag{54}$$

The resulting expression for the inverse Laplace transform in Eq. (52) is

$$h(t)*\theta_0(x,t)=\tfrac{F_0}{4k}\sum_{n=1}^{\infty}\frac{A_n(\omega_0)}{in\omega_0}\left\{e^{in\omega_0 t}\left[e^{\sqrt{in\omega_0}Q}\mathrm{erfc}\left(\tfrac{Q}{2\sqrt{t}}+\sqrt{in\omega_0 t}\right)+e^{-\sqrt{in\omega_0}Q}\mathrm{erfc}\left(\tfrac{Q}{2\sqrt{t}}-\sqrt{in\omega_0 t}\right)\right]-2\mathrm{erfc}\left(\tfrac{Q}{2\sqrt{t}}\right)\right\}. \tag{55}$$

The integrand kernel of Eq. (37) can now be formed, the integral inverted, and the thermal-wave field calculated from the operation in step (3):

$$\theta(x,t)=-\sqrt{\alpha}\frac{\partial}{\partial Q}[h(t)*\theta_0(Q,t)]. \tag{56}$$

After some algebraic manipulation and repeated use of Leibniz's rule, we obtain the following expression for the non-steady-state multifrequency thermal-wave field:

$$\begin{aligned}\theta(x,t;\omega_0)=\frac{F_0\sqrt{\alpha}}{4k\sqrt{\omega_0}}\sum_{n=1}^{\infty}\frac{A_n(\omega_0)}{\sqrt{n}}\{W[z_-^{(n)}(x,t)]\\-W[z_+^{(n)}(x,t)]\}e^{-\left(\frac{x^2}{4\alpha t}+i\frac{\pi}{4}\right)},\end{aligned} \tag{57}$$

where

$$z_\pm^{(n)}(x,t)\equiv\frac{x}{2\sqrt{\alpha t}}\pm\sqrt{in\omega_0 t}, \tag{58}$$

and the other symbols retain their prior definitions. Equation (57) is the generalization of Eq. (27), yielding the thermal-wave response to a general multifrequency periodic excitation (photo)thermal flux incident on the semi-infinite solid surface. Using Eq. (31), the non-steady-state thermal-wave field at the surface of the solid can be immediately derived in the form

$$\theta(0,t;\omega_0)=\frac{F_0\sqrt{\alpha}}{2k\sqrt{\omega_0}}\sum_{n=1}^{\infty}\frac{A_n(\omega_0)}{\sqrt{n}}\mathrm{erf}(\sqrt{in\omega_0 t})e^{i(n\omega_0 t-\pi/4)}, \tag{59}$$

which is the generalization of Eq. (30). For large values of the arguments $z_\pm^{(n)}(x,t)$, such that $t\gg t_\infty(x,\omega_0)\equiv\max[(1/\omega_0),(x^2/4\alpha)]$, the complementary error functions in Eq. (57) tend to assume their limiting values of $\mathrm{erfc}[z_+^{(n)}(x,t)]\to\mathrm{erfc}(\infty)\approx 0$ and $\mathrm{erfc}[z_-^{(n)}(x,t)]\to\mathrm{erfc}(-\infty)\approx 2$. In those limits, the following expression is obtained for the LFM thermal-wave field at steady state:

$$\theta(x,t\gg t_\infty)=\frac{F_0\sqrt{\alpha}}{2k\sqrt{\omega_0}}\sum_{n=1}^{\infty}\frac{A_n(\omega_0)}{\sqrt{n}}e^{-\sqrt{in\omega_0/\alpha}x}e^{i(n\omega_0 t-\pi/4)}. \tag{60}$$

2. Steady-state LFM thermal waves

In the special case of a LFM sweep (chirp) excitation function described by flux Eq. (42), the Fourier approach gives a complex Fourier series expansion of the flux in the form

$$f_{T_0}(t) = \frac{1}{2}F_0 e^{i(\omega_1 t + R^2 t^2)} = \sum_{n=1}^{\infty} b_n e^{in\omega_0 t}; \quad \omega_0 = \frac{2\pi}{T_0}. \quad (61)$$

We note that the Fourier series expansion is valid for time-periodic functions $0 < t < T_0$, whereas the Fourier integral is essentially aperiodic. This subtle difference becomes crucial in the case of non-steady-state versus steady-state periodic LFM waveforms. According to Eq. (6b) and the definition of the Dirac delta function given by Eq. (33), the Fourier transform of Eq. (61) is

$$\tilde{F}(\omega) = \sum_{n=1}^{\infty} b_n \delta(\omega - n\omega_0);$$
$$b_n = \frac{1}{T_0}\int_0^{T_0} f_{T_0}(t) e^{-in\omega_0 t} dt; \quad n = 1, 2, 3, \ldots. \quad (62)$$

This leads to $b_n = A_n(\omega)$, with the latter being given in Eq. (45). The temperature field, Eq. (14), now takes on the form

$$\theta(x, \omega_0) = \frac{F_0}{2k}\int_{-\infty}^{\infty}\left[\sum_{n=1}^{\infty} A_n(\omega)\delta(\omega - n\omega_0)\right] \times \left[\frac{e^{-(i\omega/\alpha)^{1/2}x}}{(i\omega/\alpha)^{1/2}}\right] e^{i\omega t} d\omega,$$
$$= \frac{F_0\sqrt{\alpha}}{2k\sqrt{\omega_0}}\sum_{n=1}^{\infty}\frac{A_n(\omega_0)}{\sqrt{n}} e^{-\sqrt{in\omega_0/\alpha}x} e^{i(n\omega_0 t - \pi/4)} \quad (63)$$

and is identical to Eq. (60), which is obtained from the considerably more involved Fourier-Laplace approach in the limit of times that are large compared with ω_0^{-1}, i.e., equivalent to very long (infinite) period. The structure of Eq. (63) is that of a linear superposition of the fundamental LFM repetition rate, ω_0, and partial thermal waves simultaneously excited at all harmonics of the fundamental, $n\omega_0$, where $n = 2, 3, \ldots$.

The LFM thermal diffusion length corresponding to Eq. (63) can be calculated from defining Eq. (22) and steady-state Eq. (60)

$$\langle x_s(\omega_0)\rangle = \frac{\int_0^{\infty} x\left|\sum_{n=1}^{\infty}\frac{A_n(\omega_0)}{\sqrt{n}} e^{-(in\omega_0/\alpha)^{1/2}x} e^{i(n\omega_0 t - \pi/4)}\right| dx}{\int_0^{\infty}\left|\sum_{n=1}^{\infty}\frac{A_n(\omega_0)}{\sqrt{n}} e^{-(in\omega_0/\alpha)^{1/2}x} e^{i(n\omega_0 t - \pi/4)}\right| dx}$$
$$\simeq \frac{\int_0^{\infty} x\sum_{n=1}^{\infty}\frac{1}{\sqrt{n}}|A_n(\omega_0)||e^{-(in\omega_0/\alpha)^{1/2}x}|dx}{\int_0^{\infty}\sum_{n=1}^{\infty}\frac{1}{\sqrt{n}}|A_n(\omega_0)||e^{-(in\omega_0/\alpha)^{1/2}x}|dx}. \quad (64)$$

Equation (64) gives the following LFM chirp TDL with repetition period T_0 at steady state:

$$\langle x_s(\omega_0)\rangle \simeq \left(\frac{2\alpha}{\omega_0}\right)^{1/2}\left[\frac{\sum_{n=1}^{\infty}\frac{|A_n(\omega_0)|}{n^{3/2}}}{\sum_{n=1}^{\infty}\frac{|A_n(\omega_0)|}{n}}\right]; \quad \omega_0 = \frac{2\pi}{T_0} \quad (65)$$

Equation (65) shows that the steady TDL is shorter than its counterpart oscillating only at the fundamental angular frequency $\omega_0 = 2\pi/T_0$, Eq. (32). This is physically as expected because over its repetition period T_0 the LFM excites partial thermal waves of a very wide harmonic frequency range, all higher than the fundamental repetition rate $\omega_0/2\pi$, thereby resulting in a contracted thermal centroid closer to the solid surface than that of the purely sinusoidal thermal wave at the fundamental frequency. When $n = 1$, the incident thermal waveform contains a single angular frequency component, ω_0 (purely harmonic limit). In this case, Eq. (65) reduces to the conventional single-frequency expression, Eq. (32), as expected.

IV. SIMULATIONS OF LFM THERMAL-WAVE FIELDS

The steady-state LFM thermal-wave field of Eqs. (60) or (63) (real part) with $T_0 = 40$ s, $f_1 = 0.1$ Hz, and $f_2 = 1$ Hz is shown in Fig. 1. Although the field is in the steady-state limit of the theory, it is clear from Fig. 1(a) that the steady state is time dependent over the waveform repetition period. This turns out to be the case, as a general rule, for LFM thermal excitation of solids. It is so because the various spectral components that comprise the overall thermal response of the solid, as a linear superposition of an infinite number of partial waves (wavelets), are not in phase with one another, a fact that results in instantaneous phase relations that depend on time, and thus, control the amplitude of the oscillation. The amplitude of each wavelet is determined by the coefficients $A_n(\omega_0)$, Eq. (45). Five such partial waves are shown in Fig. 1(b).

An important part of this work is the time to steady state from the instant a thermal source impinges on the

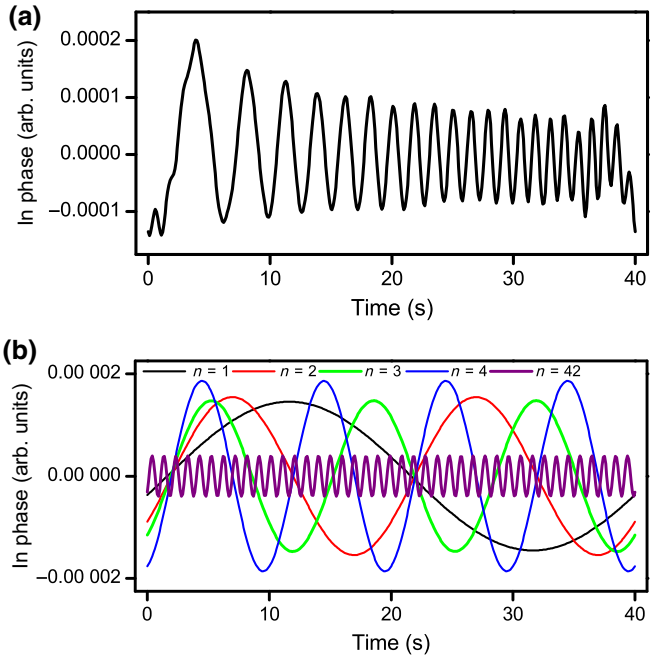

FIG. 1. (a) Steady-state LFM thermal-wave field at the surface of a semi-infinite solid with the following parameters: $T_0 = 40$ s, $f_1 = 0.1$ Hz, and $f_2 = 1$ Hz. (b) Five partial waves with $n = 1$, 2, 3, 4, and 42 of the linear superposition of the spectrum comprising the LFM thermal wave.

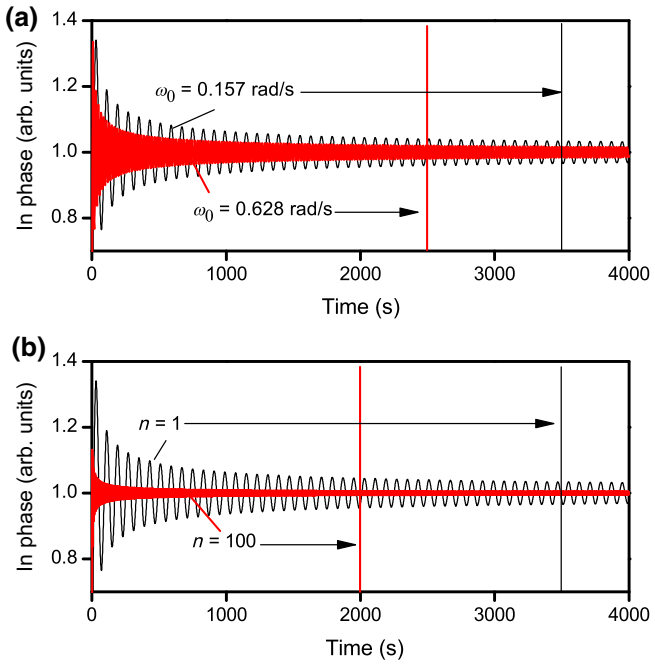

FIG. 2. (a) Time dependence of the real part of $\mathrm{erf}\left(\sqrt{i\omega_0 t}\right)$ for two values of ω_0. Vertical lines indicate attainment of steady state for each ω_0 value. (b) Time dependence of the real part of $\mathrm{erf}\left(\sqrt{i\omega_0 t}\right)$ for two values of n. Vertical lines indicate attainment of steady state for each n value.

surface of an opaque semi-infinite solid. If the incident-flux waveform is a thermal impulse, then Eqs. (21) and (23) show that there is no steady-state attainment, and the thermal diffusion length continuously increases with time. In the case of modulated thermal-wave fields, both under single-frequency and multifrequency excitation, Eqs. (30) and (59), respectively, the attainment of a steady response is controlled by the complex-argument error function. Figure 2(a) shows plots of the real part of $\mathrm{erf}\left(\sqrt{in\omega_o t}\right)$ with $n = 1$, corresponding to single-frequency thermal waves, for two values of ω_0. It can be seen that a higher angular frequency results in a faster upper limit of $\mathrm{erf}\left(\sqrt{in\omega_o t}\right)$ being attained in absolute time since the onset of the thermal oscillation. However, in terms of modulation periods T_0, the two non-steady-state thermal waves at modulation frequencies 0.025 and 0.05 Hz attain steady state in 84.8 and 166 periods, respectively. "Steady-state" time is defined as the time to reach 99% of the final value $\lim_{t\to\infty}\left|\mathrm{erf}\left(\sqrt{in\omega_o t}\right)\right| \to 1$. Figure 2(b) shows the behavior of the complex error function in non-steady-state Eq. (59) for two values of n. Again, it is observed that a larger value of n results in this function reaching steady state faster. This implies that the fundamental and other next-lowest spectral frequency components of the LFM chirp are limiting the time to steady state of the resulting thermal-wave field.

The foregoing simulations raise the important question of the number of repetition periods required for a LFM thermal-wave field in a semi-infinite solid to reach steady state, as defined here (99% of the value attained at $t\to\infty$). Figure 3 shows that the relative difference between the real part of a non-steady-state thermal-wave field ("relative in-phase difference") with surface value given by Eq. (59), and its steady-state limit, Eq. (60), reaches a steady value only after 30 periods for $\omega_0 = 0.0785$ rad/s ($T_0 = 80$ s) and after 100 periods for $\omega_0 = 0.628$ rad/s ($T_0 = 10$ s). A similar conclusion is found when single-frequency thermal-wave fields are investigated. These long time intervals should be taken into consideration and used as a guide to experimental applications when instrumental thermal-wave systems are employed for measuring material properties, as non-steady-state measurements can lead to imprecise results larger than 10% of actual values.

V. EXPERIMENTS AND RESULTS

The experimental photothermal radiometry (PTR) system used to validate the theoretical predictions is shown in Fig. 4. A Jenoptik laser diode (wavelength 808 nm, power 11.3 W) is modulated using a function generator, which produces LFM chirped waveforms with operator-controlled starting and ending frequencies and frequency scan rates. The modulated laser beam is expanded with a

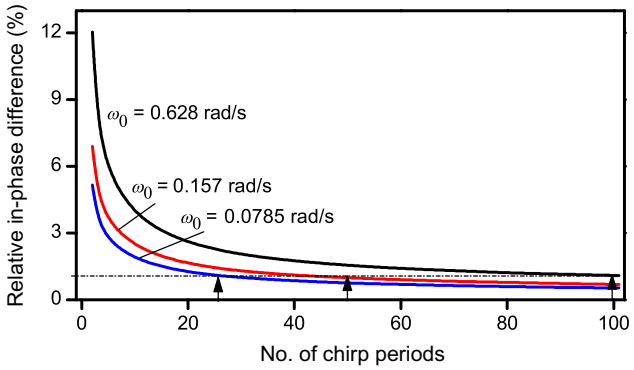

FIG. 3. Time to steady state, in units of LFM periods, of three non-steady-state thermal-wave fields with different ω_0 values.

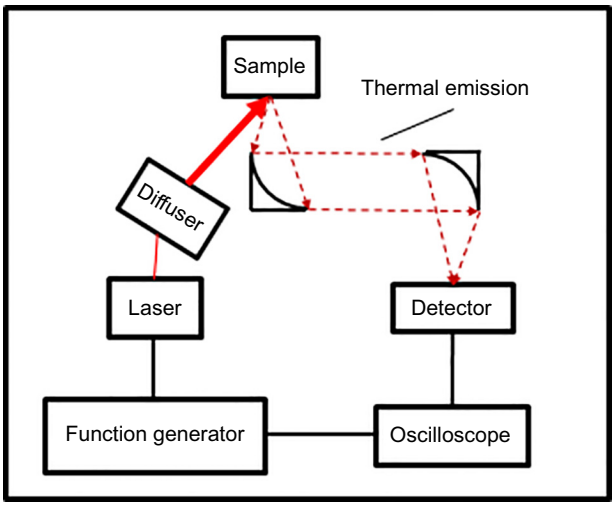

FIG. 4. Experimental PTR system.

diffuser to 3×3 cm^2 size and impinged on a 3-cm-thick anodized aluminum block acting as a surface absorber. The generated Planck thermal emission is focused on a 2–5 μm mercury cadmium zinc telluride detector (PVI-4TE-5, VIGO System S.A., Poland) through a pair of parabolic mirrors. The thermal-wave response of the solid sample is displayed on an oscilloscope triggered by the function generator. Figures 5(a) and 5(b) show the incident optical chirp waveforms (and photothermal fluxes) and the resulting surface thermal-wave oscillations recorded by the MCZT detector for two sets of experimental parameters, T_0 and R, Eq. (42b). The agreement between experimental and theoretical heat-flux traces in Figs. 5(a) and 5(b) is excellent. The experimental thermal-wave response traces in both figures were obtained after steady-state was attained. In Fig. 5(a), the response represents the steady-state in-phase component of the thermal-wave signal obtained during the 45th period, 900 s after the onset of surface laser irradiation. The respective steady-state response in Fig. 5(b) is obtained during the 175th period or 350 s after laser irradiation onset. These trends are significant in confirming and highlighting the large number of waveform repetition periods required for steady-state attainment, consistent with the temporal behavior of $\mathrm{erf}\left(\sqrt{in\omega_o t}\right)$ in non-steady-state Eq. (59) as it converges toward the steady state, Eq. (60). They are also consistent with the numbers of single-frequency thermal-wave modulation periods to steady state, Fig. 2(a). The signal-to-noise ratios (SNRs) of the experimental waveforms in Fig. 5 are seen to increase with decreasing chirp frequency ranges, as expected from the $\omega_0^{-1/2}$ relation of the amplitudes, Eq. (60). The theoretical best fits to the experimental LFM waveforms are very good, and both sets of traces exhibit the time-dependent steady-state behavior of the multifrequency responses predicted by theory. The onset of the first and last theoretical chirp oscillations in Figs. 5(a) and 5(b) diverge from the experimental thermal waveforms, probably as a result of Gibbs phenomena at the endpoints of the Fourier series representations. This effect is also visible in Fig. 1(a).

VI. DISCUSSION

The thermal diffusion length is an important parameter that characterizes the depth of penetration of modulated thermal-wave signals. For *purely transient* thermal flux waveforms, such as the thermal impulse, Eq. (20), the time-domain TDL, Eq. (23), shows the time evolution of the diffusive thermal-field penetration in the bulk of a semi-infinite solid. Conversely, for *purely harmonically modulated* thermal fluxes, Eq. (24), the baseline increase in the thermal content of the solid material due to the repeated surface thermal flux oscillation is represented by the constant term in Eq. (24) and results in the transient term $\propto 2\sqrt{t}i\mathrm{erfc}(x/2\sqrt{\alpha t})$ of thermal response Eq. (26). The usual approach here is to neglect this term when lock-in detection at the thermal flux-modulation frequency is part of the experimental implementation because lock-in demodulation eliminates the thermal transient component of the signal. In more general cases, where the thermal modulation source has a multifrequency spectrum and becomes time dependent, such as a LFM chirp, Eq. (42), there are similarities to the harmonic modulation case. In those cases, lock-in detection is not possible; however, other coherent-signal spectral analysis processing methods, such as cross correlation [25], are usually implemented to eliminate any background transients and restore an acceptable SNR for the thermal-wave response. It is for this reason that we do not include the constant term in the multifrequency thermal flux, Eq. (42a). Nevertheless, both harmonic modulation and wider-bandwidth LFM modulation result in the Fourier-Laplace convolution integral, Eq. (17), which mixes temporal components of the thermal-flux waveform with the broadened-frequency spectrum of

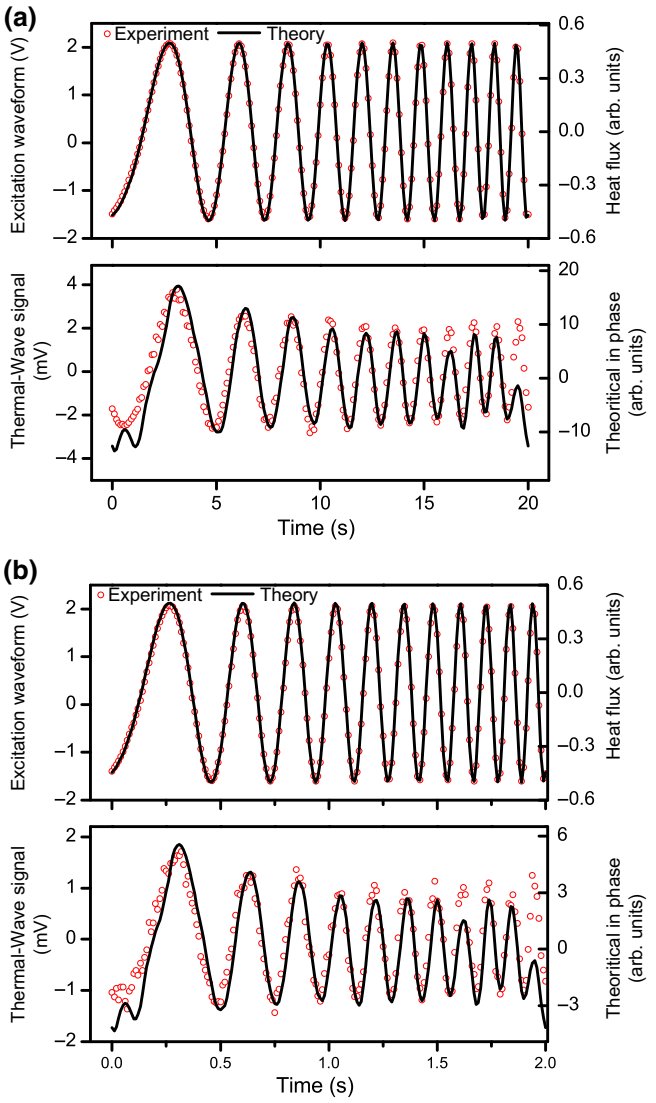

FIG. 5. (a) Thermal-wave flux and anodized aluminum sample response to a LFM chirp with parameters $f_1 = 0.1$ Hz, $f_2 = 1$ Hz, and $T_0 = 20$ s ($R = 0.376$ s^{-1}). Theoretical heat flux and steady-state in-phase response are compared with measurement results during the 45th period. (b) Thermal-wave flux and anodized aluminum sample response to a LFM chirp with parameters $f_1 = 1$ Hz, $f_2 = 10$ Hz, and $T_0 = 2$ s ($R = 3.76$ s^{-1}). Theoretical heat flux and steady-state in-phase response are compared with measurement results during the 175th period.

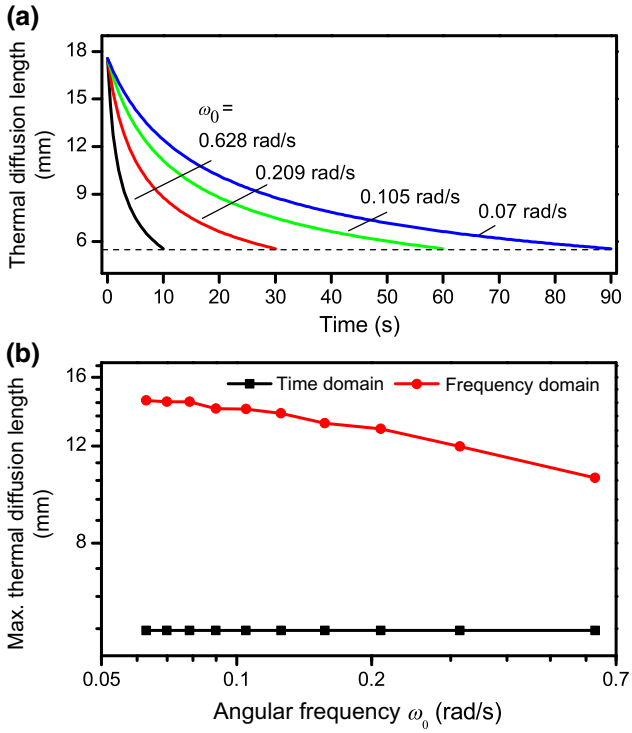

FIG. 6. Time-domain (a) and frequency-domain (b) LFM chirp thermal diffusion length comparison for aluminum. Time-domain TDL is independent of ω_0 for fixed $\Delta\omega$; frequency-domain TDL decreases with increasing ω_0.

the diffusive thermal impulse response of the solid. This physical process results in the non-steady-state response of solids described in Eqs. (27) (harmonic modulation) and (57) (LFM modulation), neither one of which can be eliminated by lock-in [26] or cross-correlation demodulation [25], respectively. Furthermore, harmonic lock-in detection can produce a truly time-independent steady-state demodulated thermal-wave amplitude and phase after several non-steady-state modulation periods, as shown by Eq. (29) and Fig. 2(a). However, this is not the case with the wider-bandwidth LFM modulation, which superposes partial waves of different phases at different times within the repetition period of the chirp, Fig. 1, thereby leading to time-dependent steady-state responses, Eq. (60) and Fig. 5, and the subsequent cross-correlation peak amplitudes and phases. Therefore, under this hybrid steady-state condition, one is faced with defining the key characteristic TDL of the repetitive LFM chirp as either a time-domain or a frequency-domain property. Mulaveesala and Tuli [11] adopted a time-dependent TDL definition of

$$\mu_{\mathrm{LFM}}(f\,;t) = \sqrt{\frac{\alpha}{\pi(f\ + Bt/\tau)}}, \tag{66}$$

where α is the thermal diffusivity of the solid, $f = \omega_1/2\pi$, and $B/\tau = \Delta\omega/2\pi T_0$, in terms of the present definitions of the LFM chirp, Eq. (42). Equation (66) has the advantage of becoming reduced to the well-known TDL Eq. (32) in the limit of harmonic modulation ($B = 0$). However, the use of Eq. (66) is not consistent with an exact solution to the LFM boundary-value problem of Eqs. (1) and (2) with $f\,(t)$ given by Eq. (42). Although an approximate solution to the foregoing boundary-value problem is presented [11], the degree of approximation is not quantified. Figure 6(a) shows the time evolution of Eq. (66) for several TDLs corresponding to different values of the angular

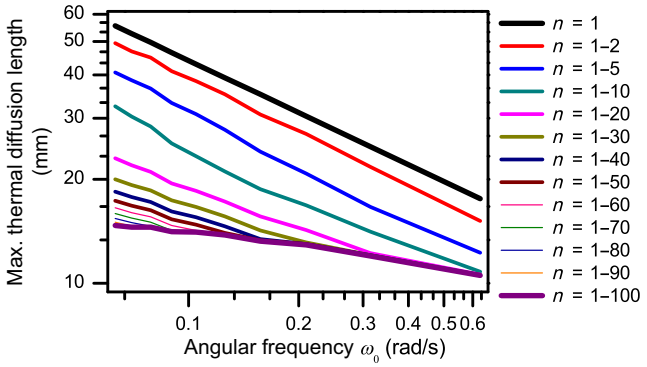

FIG. 7. TDLs of single-frequency-modulated thermal-wave field ($n=1$) and of a LFM chirp ($n=1$–100). $f_1=0.1$ Hz, $f_2=1$ Hz, $T_0=10$–100 s, and $\omega_0=2\pi/T_0=0.0628$–0.628 rad/s.

repetition rate of the chirp $\omega_0=2\pi/T_0$ by changing T_0 (from 10–90 s) for a fixed value of $\Delta\omega[=2\pi(1\text{–}0.1\text{ Hz})]$. The decay rate of each curve increases with increasing ω_0, as expected; however, the final (maximum) values of all TDLs at $t=T_0$ are the same, regardless of ω_0. This is further observed in Fig. 6(b), which also shows the frequency-domain TDL, Eq. (65). Both TDLs are consistent with the single-harmonic modulation limits of the defining equations: the time-domain LFM requires that the ending frequency f should be adjusted for varying the full depth penetration of the thermal wave, regardless of the repetition period T_0. Therefore, the time domain chirp diffusion length from Eq. (66) is a constant (flat line), while the frequency domain chirp diffusion length from Eq. (65) decreases with ω_0.

Figure 7 shows a comparison between the conventional TDL associated with thermal waves generated from single-frequency modulation in the frequency range between 0.1 and 0.7 Hz, Eq. (32), corresponding to Eqs. (32) or (65) with a single term, $n=1$, and the full LFM chirp TDL with the same repetition angular frequency, Eq. (65). The plot also shows the contributions of successive partial waves to the TDL, which saturates to the full multifrequency chirp TDL with the infinite bandwidth of higher harmonics of fundamental frequency $f=1/T_0$ in the $n\sim100$ range for the lowest frequency of 0.01 Hz. Higher fundamental frequencies require fewer n terms, as the partial thermal wavelengths of the spectrum become shorter, and thus, add negligible contributions to the full TDL. The TDL resulting from the full superposition of partial waves with $n\geq1$ decreases with increasing ω_0, as intuitively expected from faster LFM chirps sampling shallower subsurface depths. For the parameters of these particular LFMs, the chirp TDLs are several times shorter than the respective single-frequency TDL due to the superposition (mixing) of all orders of the higher harmonics. This is an important property of LFM probes, especially for imaging applications, when implemented with midinfrared cameras, for example, in the case of dynamic thermal-wave radar imaging [27]. The considerably shorter TDLs of LFM chirp waveforms than those of single-frequency probing can yield more spatially localized and better lateral and radial resolution from a range of subsurface depths. In imaging, single-frequency probing at the same TDL would require much higher modulation frequencies and frame rates, which are usually unavailable in present-day mid-IR cameras. This important advantage of LFM thermal-wave radar imaging, compared with conventional lock-in thermography is also confirmed experimentally [13].

VII. CONCLUSIONS

We introduce a combined Fourier-Laplace formalism based on the frequency spectrum of thermal fields generated in solids by arbitrary time-dependent boundary surface flux conditions as a universal approach to defining generalized non-steady-state transient (thermal) responses and modulated thermal waves. For single-frequency and multifrequency modulated thermal-wave fields, we show that the Fourier-Laplace formalism provides a passage to the modulated steady state in the limit of infinite repetition period of the excitation waveform, consistent with a purely Fourier domain spectral approach, while setting the conditions for attainment of the steady state in terms of numbers of excitation waveform repetition periods. The spectral theory is applied to LFM chirp thermal excitation waveforms associated with thermal-wave radar imaging. We find both theoretically and experimentally, using photothermal radiometry responses from anodized aluminum, that steady-state LFM is time dependent. The spectral theory is further used to define the TDL associated with steady-state LFM thermal-wave fields in terms of linear superpositions of partial thermal waves.

ACKNOWLEDGMENTS

The authors are grateful to the Natural Sciences and Engineering Research Council of Canada (NSERC), for a Discovery grant to A.M., and to the Canada Research Chairs program.

[1] Allan Rosencwaig and Allen Gersho, Theory of the photoacoustic effect with solids, J. Appl. Phys. **47**, 64 (1976).
[2] Alan F. McDonald and Grover C. Wetsel, Jr., Generalized theory of the photoacoustic effect, J. Appl. Phys. **49**, 2313 (1978).
[3] Andreas Mandelis and Barrie S. H. Royce, Time-domain photoacoustic spectroscopy of solids, J. Appl. Phys. **50**, 4330 (1979).
[4] Yoh-Han Pao, *Optoacoustic Spectroscopy and Detection* (Academic, New York, 1977).

[5] Allan Rosencwaig, *Photoacoustics and Photoacoustic Spectroscopy* (Wiley, New York, 1980).
[6] Vitalyi E. Gusev and Alexander A. Karabutov, *Laser Optoacoustics (Transl. K. Hendzel* (AIP, New York, 1993).
[7] Andreas Mandelis, Frequency modulated (FM) time delay photoacoustic and photothermal wave spectroscopies. technique, instrumentation and detection. part I: Theoretical, Rev. Sci. Instrum. **57**, 617 (1986).
[8] Andreas Mandelis, Linda M.L. Borm, and John Tiessinga, Frequency modulated (FM) time delay photoacoustic and photothermal wave spectroscopies. technique instrumentation and detection. part II: Mirage effect spectrometer, design and performance, Rev. Sci. Instrum. **57**, 622 (1986).
[9] Andreas Mandelis, Linda M.L. Borm, and John Tiessinga, Frequency modulated (FM) time delay photoacoustic and photothermal wave spectroscopies. technique instrumentation and detection. part III: Mirage effect spectrometer, dynamic range and comparison to pseudo random binary sequence (PRBS) method, Rev. Sci. Instrum. **57**, 630 (1986).
[10] Nima Tabatabaei and Andreas Mandelis, Thermal-wave radar: A novel subsurface imaging modality with extended depth-resolution dynamic range, Rev. Sci. Instrum. **80**, 034902 (2009).
[11] Ravibabu Mulaveesala and Suneet Tuli, Theory of frequency modulated thermal wave imaging for nondestructive subsurface defect detection, Appl. Phys. Lett. **89**, 191913 (2006).
[12] Ravibabu Mulaveesala, Vaddi J. Somayajulu, and Pushpraj Singh, Pulse compression approach to infrared nondestructive characterization, Rev.Sci. Instrum. **79**, 094901 (2008).
[13] Nima Tabatabaei and Andreas Mandelis, Thermal Coherence Tomography Using Match Filter Binary Phase Coded Diffusion Waves, Phys. Rev. Lett. **107**, 165901 (2011).
[14] Sreekumar Kaiplavil and Andreas Mandelis, Truncated-correlation photothermal coherence tomography for deep subsurface analysis, Nat. Photonics **8**, 635 (2014).
[15] Fei Wang, Yonghui Wang, Junyan Liu, and Yang Wang, Optical excitation fractional Fourier transform (FrFT) based enhanced thermal-wave radar imaging (TWRI), Opt. Express **26**, 21403 (2018).
[16] Hamed Malekmohammadi, Stefano Laureti, Pietro Burrascano, and M. Ricci, Comparison of optimisation strategies for the improvement of depth detection capability of pulse-compression thermography, Quant. Infrared Thermogr. J. (2019).
[17] Ghali V. Subarao and Ravibabu Mulaveesala, Quadratic frequency modulated thermal wave imaging for non-destructive testing, Progr. Electromag. Res. M **26**, 11 (2012).
[18] Ravibabu Mulaveesala, Geetika Dua, and Vanita Arora, Applications of Infrared Thermography for non-Destructive Characterization of Concrete Structures, in Advances in Structural Health Monitoring IntechOpen (2019); Shaik Subhani, Gampa V. P. C. Sekhar Yadav and Venkata S. Ghali, Defect characterisation using pulse compression-based quadratic frequency modulated thermal wave imaging, IET Sci. Meas. Technol. **14**, 165 (2020).
[19] Andreas Mandelis, *Diffusion-Wave Fields: Mathematical Methods and Green Functions* (Springer-Verlag, New York, 2001).
[20] Horatio S. Carslaw and John C. Jaeger, *Conduction of Heat in Solids*, 2nd Ed. (Oxford Univ. Press, Oxford, 1959), p. 76, Eq. (2.9.9).
[21] Philip R. Wallace, *Mathematical Analysis of Physical Problems* (Dover, Mineola, N.Y., 1984), pp. 187–188.
[22] Larry C. Andrews and Bhimsen K. Shivamoggi, *Integral Transforms for Engineers* (SPIE Opt. Eng. Press, Bellingham, WA, 1999), Sect. 4.1.
[23] Anatolij P. Prudnikov, Ûrij A. Brychkov and Oleg I. Marichev, *Integrals and Series, Vol. 5: Inverse Laplace Transforms* (Gordon & Breach, New York, 1992).
[24] Andreas Mandelis and Zhuohui Chen, Lock-in rate-window thermomodulation (thermal wave) and photomodulation spectrometry, Rev. Sci. Instrum. **63**, 2977 (1992).
[25] Julius S. Bendat and Allan G. Piersol, *Engineering Applications of Correlation and Spectral Analysis* (Wiley-Interscience, New York, 1980).
[26] A. Mandelis, Signal-to-noise ratio in lock-in amplifier synchronous detection: A generalized communications systems approach with applications to frequency, time, and hybrid (rate window) photothermal measurements, Rev. Sci. Instrum. **65**, 3309 (1994).
[27] Nima Tabatabaei, Andreas Mandelis, and Bennett Amaechi, Thermophotonic radar imaging: An emissivity-normalized modality with advantages over phase lock-in thermography, Appl. Phys. Lett. **98**, 163706 (2011).